

# NESTED BARS IN DISK GALAXIES: NO OFFSET DUST LANES IN SECONDARY NUCLEAR BARS

Isaac Shlosman<sup>1,2</sup>

*Joint Institute for Laboratory Astrophysics, University of Colorado, Box 440, Boulder, CO 80309-440*  
*email: shlosman@pa.uky.edu*

and

Clayton H. Heller

*Department of Physics, Georgia Southern University, Statesboro, GA 30460-8031*  
*email: cheller@gasou.edu*

## ABSTRACT

Under certain conditions, sub-kpc nuclear bars form inside large-scale stellar bars of disk galaxies. These secondary bars spend a fraction of their lifetime in a *dynamically-decoupled* state, tumbling in the gravitational field of the outer bars. We analyze the flow pattern in such nested bar systems under the conditions of negligible self-gravity and find that secondary bars differ fundamentally from their large-scale counterparts, in gas flow pattern and other dynamical properties. In particular the gas flow across the bar-bar interface in these systems can be more chaotic or more regular in nature, and, contrary to predictions, has no difficulty in penetrating the secondary bars along the primary large-scale shocks. The outer parts of both short and long nuclear bars (with respect to their corotation) appear to be depopulated of gas, while deep inside them the flow exhibits low Mach numbers and follows ovally-shaped orbits with little dissipation. Long nuclear bars remain gas-rich longer, and for this, relatively short, period of time are largely of a rectangular shape, again with a small dissipation. We find that gas-dominated and star-dominated nuclear bars avoid the bar-bar interface, making both types of bars short relative to their corotation. Furthermore, our earlier work has shown that *dynamically-coupled* secondary bars exhibit a similarly relaxed low-dissipation flow as well. Therefore, no large-scale shocks form in the nuclear bars, and consequently, no offset dust lanes are expected there. We find that offset dust lanes cannot be used in the search for secondary (nuclear) bars. Finally, we discuss the importance of gas self-gravity in the further evolution of these systems.

*Subject headings:* galaxies: evolution – galaxies: ISM – galaxies: kinematics & dynamics – galaxies: starburst – galaxies: structure – hydrodynamics

---

<sup>1</sup>JILA Visiting Fellow

<sup>2</sup>permanent address: Department of Physics and Astronomy, University of Kentucky, Lexington, KY 40506-0055

## 1. Introduction

Double bars appear to be frequent among disk galaxies, probably in excess of 20-25% (e.g., Friedli et al. 1996; Erwin & Sparke 1999; Laine et al. 2001). About 1/3 of barred galaxies host a second bar (Laine et al.). They consist of large-scale stellar (primary) bars and sub-kpc (secondary) nuclear bars. Examples of such systems have been known since de Vaucouleurs (1974), Sandage & Brucato (1979) and Kormendy (1983), although they had attributed the twisting of the innermost isophotes to a triaxial bulge. Dynamical consequences of nested bars for the stellar and gas dynamics in disk galaxies have been studied both theoretically and numerically, but are far from being understood (Shlosman, Frank & Begelman 1989; Pfenniger & Norman 1990; Friedli & Martinet 1993; Combes 1994; Heller & Shlosman 1994; Maciejewski & Sparke 2000). They have been also implicated in the fueling of active galactic nuclei and starburst activity in the central kpc (Shlosman, Begelman & Frank 1990; Athanassoula 1994; Friedli 1999).

One of the most interesting aspects of nested bars is their dynamically decoupled phase, when the rate of tumbling of each bar is different. Shlosman et al. (1989) have shown that self-gravitating gas instabilities within the central kpc can be the prime reason for this runaway process, which was confirmed in numerical simulations (Friedli & Martinet 1993, Combes 1994; Heller & Shlosman 1994; Shlosman 2001). Furthermore, Shaw et al. (1993) and Knapen et al. (1995b; see also Shlosman 1996) have studied gas accumulation in the vicinity of the inner Lindblad resonance of large-scale primary bars which manifested itself in the formation of gaseous and stellar secondary bars still *coupled* to the background potential and tumbling with the primary bar pattern speed. Pfenniger & Norman (1990) used weakly dissipative equations of motion for a test particle in a double bar potential. Heller, Shlosman & Englmaier (2001) found that the formation and decoupling of the secondary gaseous bar is possible even in the limit of weak self-gravity in the gas. Finally Maciejewski & Sparke (2000) have invoked multi-periodic (loop) orbits to support the time-dependent gravitational potential of a double bar system.

Detection techniques of secondary bars depend on the type of the bar, namely gaseous or stellar. The stellar bars have been found using photometry, most efficiently in the optical and NIR (e.g., Scoville et al.

1988; Buta & Crocker 1993; Knapen et al. 1995a; Shaw et al. 1995; Friedli et al. 1996; Jungwiert, Combes & Axon 1997; Erwin & Sparke 1999; Knapen, Shlosman & Peletier 2000; Laine et al. 2001). The gaseous molecular bars have been observed using CO and H<sub>2</sub> (e.g., Ishizuki et al. 1990; Devereux, Kenney & Young 1992; Maiolino et al. 2000; Sakamoto, Baker & Scoville 2000). Recently Regan & Mulchaey (1999) and Martini & Pogge (1999) have invoked the so-called offset dust lanes to compare the frequency of secondary bars in Seyferts and ‘normal’ galaxies, using high-resolution HST imaging. Such offset lanes are routinely detected in large-scale bars and represent global (collisional) shocks in the ISM, in response to torquing by the bar potential. Extensive numerical study has revealed the close connection between the shape of these dust lanes, mass distribution in the galaxy, strength of the stellar bar and its pattern speed (Athanassoula 1992).

In this paper we analyze the gas dynamics in dynamically-decoupled secondary nuclear bars and show that the gas response to their torquing is fundamentally different from that of their large-scale counterparts. This leads to a number of theoretical and observational consequences. Our results clarify the details of gas flow across the bar-bar interface and within the secondary bar. We find that no large-scale shocks and offset dust lanes can form in the nuclear bars. Dust lanes, therefore cannot be used to search for nested bar systems, in general, and, specifically, cannot address the issue of morphological differences between Seyfert and normal host galaxies.

## 2. Model Construction and Orbit Analysis

### 2.1. Orbits in single and nested bars

To study the gas flow in the nested bar systems, we constructed a grid of models, with two representative cases analyzed below. We use the 2-D version of our Smooth Particle Hydrodynamics (SPH) code (Heller & Shlosman 1994) in the background potentials of both bars embedded in the disk and spheroidal components, neglecting the gas self-gravity. This code has a dynamic spatial resolution which is defined by the kernel smoothing length. An SPH neighborhood of 96 gas particles was used.

In this section we define the model potentials, examine the orbits they support and verify the positions of inner resonances in the disk by means of nonlinear orbit analysis (see Heller & Shlosman 1996 for

technical details). This is important because these resonances not only describe the distribution of main families of periodic stellar orbits but provide an insight into the gas response to nested bar torquing.

Two resonances, corotation and the inner Lindblad resonance(s)<sup>3</sup> (ILRs), play a special role in the evolution of disk galaxies with *single* bars. Two families of periodic orbits are dominant within the bar corotation. The first family, so-called  $x_1$ , is aligned with the bar and extends between the center and the corotation radius (Contopoulos & Papayannopoulos 1980). The second family,  $x_2$ , is found between the ILRs and its orbits are oriented perpendicular to the bars major axis. These latter orbits weaken the bar when they are populated.

Both  $x_1$  and  $x_2$  families are resonant orbits which tumble with the bar pattern speed. Each of these orbits corresponds to a fixed Jacobi energy,  $E_J$ , which is a constant of motion along the orbit in the rotating frame of the bar (e.g., Binney & Tremaine 1987). The orbital shapes do change with  $E_J$ .

Gas orbits of course do not follow exactly either of the two main families of orbits because of internal dissipation and do not conserve  $E_J$ . This energy non-conservation is amplified further for orbits with loops or pointed ends, in which case shocks develop and the gas rapidly depopulates them. In the bar frame of reference the gravitational potential of a single-barred galaxy is time independent, which makes it easier to describe the gaseous response. Unlike the stellar orbits which can change their response abruptly at each resonance, from being aligned with the bar to being perpendicular, and vice versa, the gas responds gradually and its orbits change their orientation by forming a pair of offset shocks. These shocks have been detected by the dust lanes, whose shape is constrained by the ratio of corotation-to-bar-radii,  $1.2 \pm 0.2$ , as found empirically by Athanassoula (1992).

In the *nested* bar galactic systems, when both bars are dynamically decoupled and tumble with different pattern speeds, the gravitational potential is time-dependent in all frames of reference. In such a case Jacobi energy is not an integral of motion even for the collisionless ‘fluid,’ i.e., stars. One can look for an alternative treatment such as the one proposed by Maciejewski & Sparke (2000) who introduced multi-periodic orbits, called ‘loops,’ supporting the double

bar system. However, it is not clear what fraction of the phase space is occupied by these loops and how many orbits are actually trapped around them. In any case these orbits are not suitable for the gas, as all of them are intersecting.

In order to understand the gas flow in a nested bar potential, we analyze the main families of periodic orbits in the frames of reference of each of the bars, with the other bar being symmetrized. This allows one to interpret the observed gas response in the numerical simulations of these systems, albeit roughly.

A number of rules need to be followed in order to construct a self-consistent nested bar system. First, a necessary condition is to accumulate a critical mass of gas, which initiates the runaway. Although in this work we assume a system already in a decoupled state, it still requires the existence of an ILR in the primary bar for consistency. This constrains the pattern speed of the primary bar. Second, the corotation radius of the secondary bar must be found in the vicinity of the above ILR, in order to decrease the fraction of chaotic orbits generated at each resonance. This fixes the pattern speed of the secondary bar. Third, the length of a secondary bar cannot exceed its corotation, but unlike in the primary bars, it can be substantially smaller. This length is determined by the amount of dissipation in the gas at the time of gas settling inside the ILR on the  $x_2$  orbits and its subsequent dynamical runaway. The details of this process are outside the scope of this paper (see e.g., Heller et al. 2001; Shlosman 2001; and in preparation).

## 2.2. Building the model

Following the above constraints, we have chosen two models which differ mainly due to the length of the secondary bar. Model 1 has a relatively short secondary bar, confined well inside its corotation (and the ILR of the primary bar). Model 2 hosts a secondary bar extending to its Ultra-harmonic resonance, which is located at about 0.83 of its corotation radius and is typical of the primary or single bars, as discussed in Section 1.

The disk and bulge/halo potential which is identical for both models is given by a Miyamoto & Nagai (1975) analytical model,

$$\Phi = -\frac{GM}{\sqrt{r^2 + (A+B)^2}}, \quad (1)$$

where  $M$  — mass in units of  $10^{11} M_\odot$  and  $A+B$  —

<sup>3</sup>The ILRs are resonances between the stellar orbital precession frequency and the bar pattern speed.

scaling parameters representing the disk radial scale-length, in units of 10 kpc (Table 1). Each bar is represented by Ferrers (1877) potential with  $n = 1$ , with the primary bars being identical in both models. In dimensionless units, nested bar masses and semi-major ( $a$ ) and semi-minor ( $b = c$ ) axes are given in Table 2. The axial ratio for the primary and secondary bars is  $b/a \sim 1 : 3$  and  $1:4$ , respectively, which corresponds to moderately strong to strong bars. The dynamical time at 10 kpc,  $\tau_{\text{dyn}} = 1$ , corresponds to  $4.7 \times 10^7$  yrs.

In both models presented here the primary bar ends at  $r \approx 0.65$ , just inside its Ultra-Harmonic resonance at 0.7. The corotation radius of the secondary bar, as discussed above, lies near the outer ILR of the primary bar, 0.09 and 0.10, for Models 1 and 2. Finally, each bar comprises about 20% of the total mass *within their respective radii*. Initially, the gas is distributed exponentially, with a scalelength of 0.3, and its sound speed is  $15 \text{ km s}^{-1}$ .

For comparison, we also present Model 3, whose radial mass distribution is identical to that of Model 1, but with an axisymmetrized secondary bar. Dynamical effects of secondary bars are emphasized this way.

### 2.3. Nonlinear orbit analysis

The choice of the primary bar pattern speed,  $\Omega_p = 1.0$ , and mass distribution has led to a double ILR in all models. The existence and positions of these resonances was verified using nonlinear orbit analysis. Fig. 1a which is the characteristic diagram for both Models 1 and 2 in the frame of reference of the primary bar,  $\Omega_p$ , allows one to understand the degree of orbital support for this bar. The  $x_1$  orbits extend from the center till the corotation, while the  $x_2$  orbits are limited between the ILRs. For a fully developed secondary bar, the inner ILR is basically located at the very center of the disk, at  $r \sim 0.008$  along the x-axis (0.01 along the y-axis), i.e., its dynamical effect is not important here. Instead, we expect the perturbation of the secondary bar to dominate the

Table 1: Model Potential Parameters

| Component | Mass | A    | B    |
|-----------|------|------|------|
| disk      | 0.6  | 0.2  | 0.05 |
| bulge     | 0.03 | 0.01 | 0.02 |
| halo      | 1.0  | 0.0  | 1.0  |

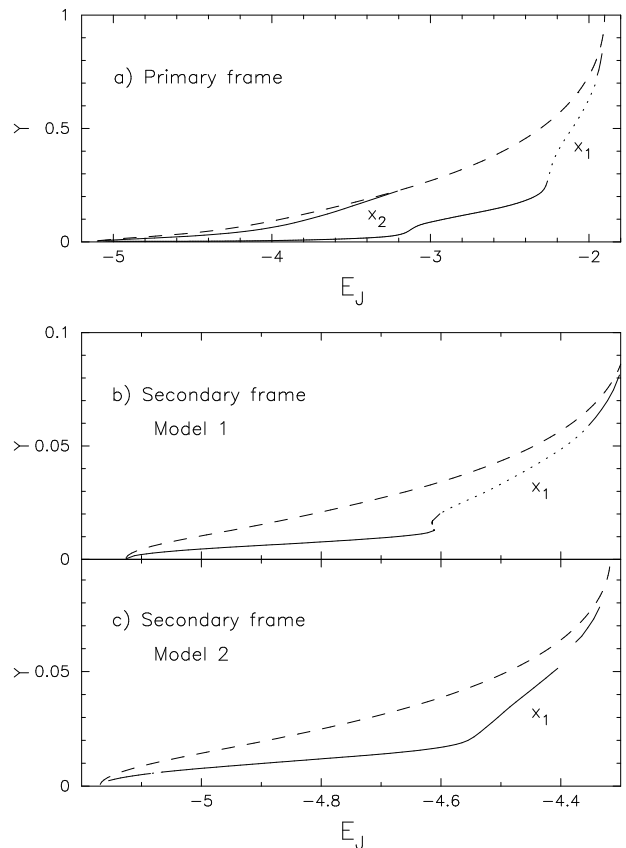


Fig. 1.— Characteristic  $x_1$  and  $x_2$  orbit diagram for Model 1 (top, middle) and Model 2 (lower). The upper panel (a) gives the orbit analysis in the frame of the primary bar, with the secondary bar being axisymmetrized. The middle (b) and lower (c) panels give the analysis in the frame of the secondary bar with the primary bar axisymmetrized. The dashed line is the zero velocity curve. The dotted line represents unstable  $x_1$  orbits. The galactic center is on the left.

dynamics at these radii. At the same time the outer ILR of the primary bar is found along the primary bar major (minor) axis at  $\approx 0.08$  ( $0.10$ ) (Model 1), and at  $\approx 0.09$  ( $0.24$ ) (Model 2). To estimate the location

Table 2: Ferrers Bar Parameters ( $n = 1$ )

| Model | Bar       | Mass  | $a$   | $b$    | $\Omega$ (bar) |
|-------|-----------|-------|-------|--------|----------------|
| 1     | primary   | 0.15  | 0.65  | 0.22   | 1.0            |
|       | secondary | 0.007 | 0.05  | 0.0125 | 8.3            |
| 2     | primary   | 0.15  | 0.65  | 0.22   | 1.0            |
|       | secondary | 0.012 | 0.075 | 0.0187 | 8.3            |

of the primary ILR, the secondary bar was axisymmetrized.

The characteristic diagrams presented in Fig. 1, especially those in the frame of reference of the secondary bar, hint about the gas response observed in our numerical simulations. No  $x_2$  orbits exist in the frame of reference of the secondary bar which tumbles fast enough to avoid its ILRs (Figs. 1b,c). In Fig. 1b (Model 1), a shoulder in the  $x_1$  characteristic is visible. Note that a broad range of these orbits at higher Jacobi energies is unstable, the exact reason for which will be discussed elsewhere. Moreover, these unstable orbits intersect with the  $x_1$  orbits at lower energies (deeper inside the bar), which corresponds to spatial scales outside  $r \sim 0.03$ . This itself means that the gas will not be able to settle down in the outer half of the secondary bar in Model 1.

The corresponding characteristic diagram produced for Model 2 (Fig. 1c) is very different. First, no shoulder exists in the  $x_1$  characteristic, which are non-intersecting and stable all the way till the corotation of this bar. One would expect the gas to fill up completely the secondary bar under these conditions. This indeed happens (Section 3) before the gas is driven further inwards due to the time-dependent potential. The overall difference between Models 1 and 2 is due to the larger quadrupole moment of longer secondary bar in the latter Model, which extends up to the Ultra-harmonic resonance, near its corotation.

### 3. Model Evolution: Gas Flow in Nested Bars

To avoid transients, the nonaxisymmetric potential is turned on gradually. The resulting gas response to the nested bar potential in both models can be best inferred by defining three regions in the disk. Namely, (i) that of the primary bar (outside its ILR region), (ii) the bar-bar interface (hereafter the *interface*) encompassing the outer ILR of the large bar and the outer part of the secondary bar, and (iii) the interior of the secondary bar.

In the first region, the primary bar outside the interface, the gas responds by forming a pair of large-scale shocks, corresponding to the offset dust lanes, and flowing inwards across the interface into the secondary bar, for Models 1 and 2, while stagnating in Model 3. During most of the evolution, the flow in the primary bar, outside the interface, is steady and the shock strength and shape are nearly independent of

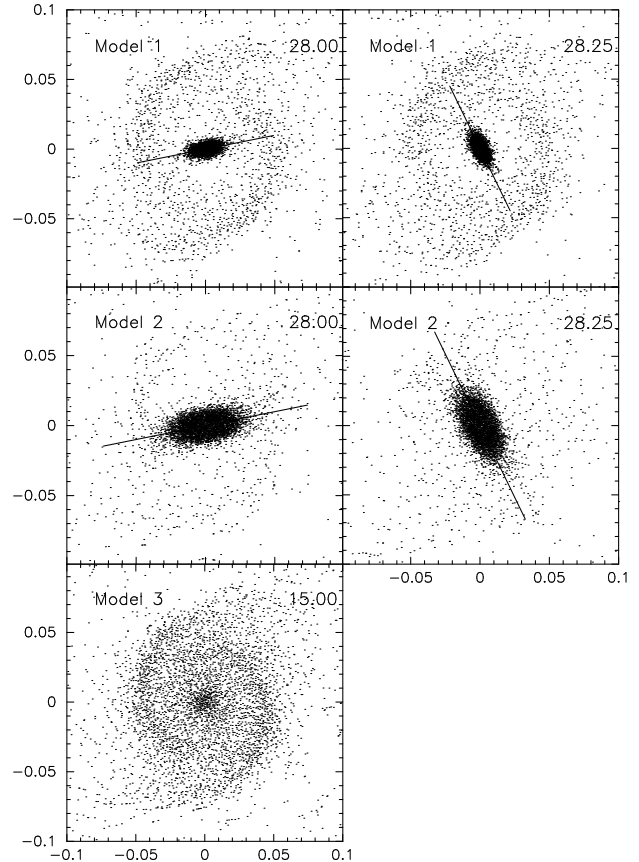


Fig. 2.— Time evolution of the gas density distribution in the central kpc ( $r = 0.1$ ) in Models 1–3: 2D SPH simulation in the background gravitational potential of a nested bar disk galaxy (face-on). The gas response to the nested bar torquing is shown in the primary bar (horizontal) frame of reference. Both bars and gas rotate counter-clockwise. The position angle of the secondary bar and its length are indicated by a straight line. Time is given in units of dynamical time  $\tau_{dyn}$ . Note the absence of a nuclear ring in Model 2.

time. This quasi-steady state exists after  $t \sim 10$  and till the end of the numerical simulations at  $t = 30$ . Our subsequent analysis is limited to this time only.

In the second region, the bar-bar interface, the flow has a time-dependent character due to the perturbative effects of the secondary bar and changing background potential, and naturally correlates with the position angle of the secondary bar with respect to the primary bar, especially in Model 2 due to a more

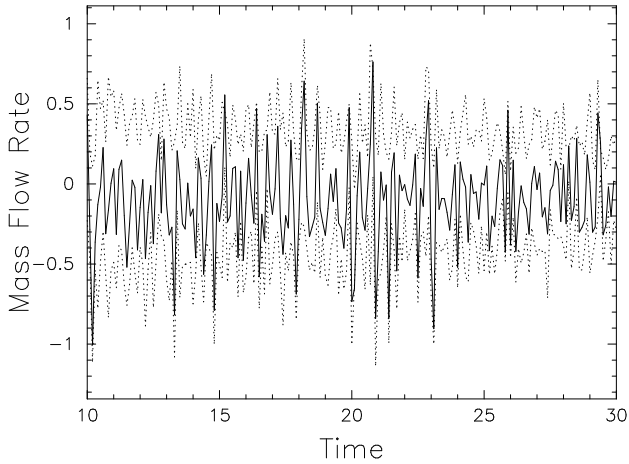


Fig. 3a.— Time evolution of the gas inflow (negative) rate across the bar-bar interface,  $r = 0.1$  (i.e., corotation of the secondary bar), of a double bar system (Model 2). *Upper dotted line*: flow rate within  $\pm 45^\circ$  of the major axis of the primary bar. *Lower dotted line*: flow within  $\pm 45^\circ$  of the minor axis of the primary bar. *Solid line*: total flow across the bar-bar interface. Time is given in units of dynamical time  $\tau_{dyn}$ .

pronounced small-scale bar (Fig. 2). To get some insight into the flow across this zone, and specifically across the corotation of the secondary bar, we have subdivided the azimuthal dependence of the gas flow into  $\pm 45^\circ$  with the major axis of the primary bar and  $\pm 45^\circ$  with its minor axis (Fig. 3a). We have Fourier analyzed the time dependence of the mass inflow rates and found the trace of the beat frequency of the secondary bar in Model 1, which in the frame of the primary bar should appear at  $f \sim 2.3$  and shows up at 2.23 (Fig. 3b), although other frequencies have substantial power as well. Model 2, having a stronger bar influence at the interface, exhibits a higher Fourier amplitude at exactly the beat frequency  $f = 2.3$ , clearly identified with the secondary bar tumbling and with less power from other frequencies.

So the flow across the bar-bar interface depends upon the strength of the secondary bar. It ranges from more chaotic, for a relatively weak perturbation of the secondary bar in Model 1, to a more regular one in Model 2. The corresponding mass influx rate is of the order of  $0.3 M_{gas,9} M_\odot \text{ yr}^{-1}$ , where  $M_{gas,9}$  is the

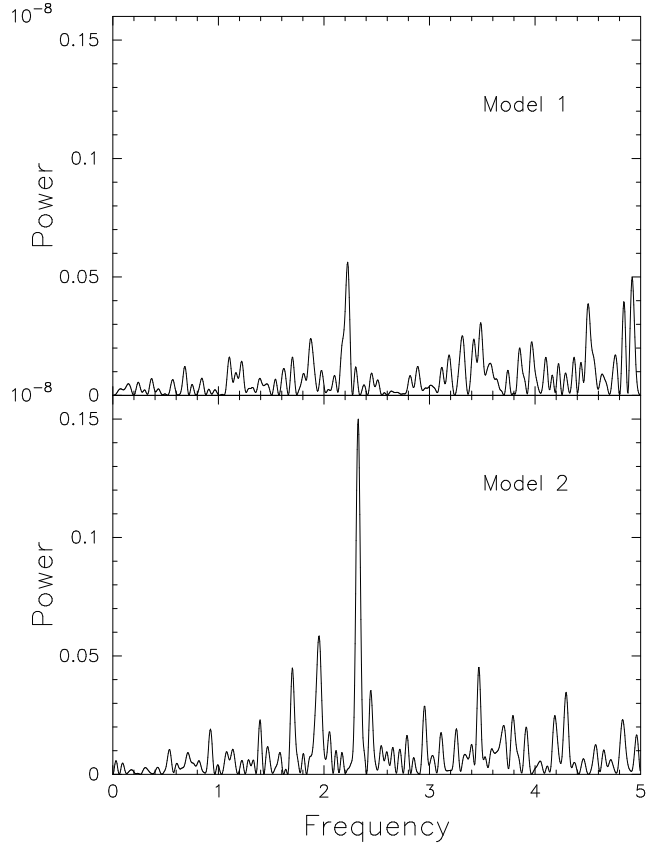


Fig. 3b.— The Fourier transform of the total gas inflow rate across the bar-bar interface,  $r = 0.1$ . Significant power at the beat frequency of the two bars,  $f \sim 2.3$ , can be seen for Model 2. Model 1 also exhibits this beat but with substantially less power, along with additional power at higher frequencies.

total gas mass in the disk in units of  $10^9 M_\odot$ . On the average, the inflow proceeds through the broad region along the primary bar minor axis, while an outflow (albeit at a smaller rate) is directed along its major axis. The reason for this behavior is that the inflow is driven mainly along the large-scale shocks penetrating the bar-bar interface from the primary bar. At the same time the outflow is detected at angles which do not encompass the large-scale shocks. The net effect is clearly an inflow across the corotation of the secondary bar, as indicated in Fig. 3a.

As a caveat, gas, which is repelled by the secondary bar along the major axis of the primary bar, is found to enter large-scale shocks while still moving out. This should aggravate, at least in princi-

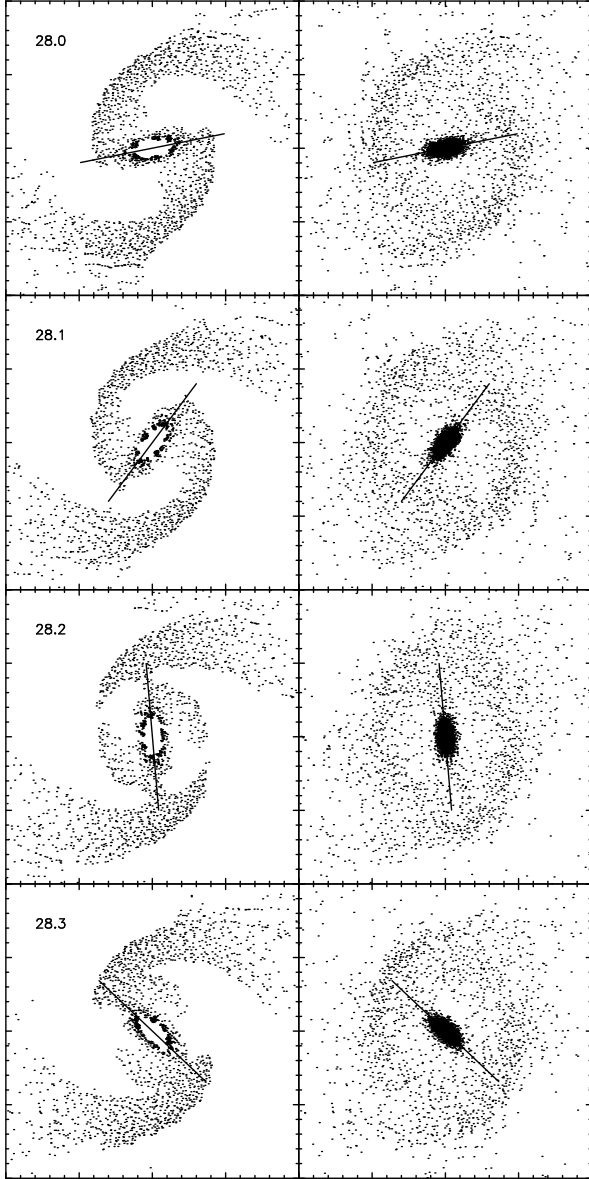


Fig. 4a.— Pattern of shock dissipation (left) and density evolution (right) in the central kpc ( $r = 0.1$ ) of Model 1, shown in the frame of reference of the primary bar (horizontal). Positions of the secondary bar and its length are indicated by a straight line. All rotation is counter-clockwise. The particles on the left are those having greater than average dissipation rate which is given by the time derivative of the nonadiabatic component of internal energy. Note the sharply reduced dissipation in the innermost 0.02 and “limb brightening” enveloping it. Also visible are two dissipative systems associate with the large-scale shocks in the primary bar and with the trailing shocks in the secondary bar.

ple, the mixing of material with a different angular momentum. Such mixing will lead to an increased inflow along the shocks and even less rotational support upon the entrance to the secondary bar. No attempt was made to quantify this effect.

The gas response at the interface and at smaller radii differs substantially among all three models. As expected, the single bar Model 3 shows no signs of further gas evolution which stagnates in the vicinity of the ILR in a nuclear ring. Fig 2 displays a single frame of gas distribution for this model at  $t = 15$ , which is also characteristic of later times. Hence we have refrained from showing other frames. This is not the case for models with secondary bars which drive the gas inward, towards smaller radii as can be seen from Fig. 2. The gas from the primary bar is crossing the bar-bar interface along the large-scale shocks, settling well inside the nuclear bar whose length is indicated by the straight line. Specifically, it falls towards the third region, within  $r < 0.02$  (Model 1) and  $< 0.04$  (Model 2). This region shows a very relaxed flow at all times, with uniform dissipation (well below the maximum dissipation in the large-scale shocks), and no evidence for grand-design shocks.

An important difference between Models 1 and 2 is the absence of a nuclear ring in the latter model. While Model 1 shows a well developed ring at all times, made out of two tightly wound spirals (Fig. 4a, right column). Model 2 develops a pair of open spiral shocks, but only when the bars are closely aligned (Fig. 4b, right column).

In order to understand the pattern of shock dissipation in nested bars, we show the time evolution of the gas which has more than the average dissipation rate within the central kpc ( $r = 0.1$ ) at different times (Figs. 4). This scale allows one to separate the incoming large-scale shocks from those driven by the secondary bar.

We first note that two systems of spiral shocks occur in Models 1 and 2, each associated with their corresponding bar. The large-scale (hereafter ‘primary’) shocks, which have been discussed above, normally extend to the minor axis of the primary bar in both Models 1 and 2, e.g., Fig. 4a at  $t = 28.2$ , Fig. 4b at  $t = 12.2$ , or Fig. 4c at  $t = 28.1$ . At these times the secondary bar is nearly orthogonal to the primary one. As it continues to tumble, the primary shocks extend deeper into the small bar. Sometime before both bars are perpendicular, the outer shocks detach from the small bar, which is left with additional pair of trail-

ing shocks. This effect is especially pronounced in Fig. 4a between  $t = 28.1$  and  $28.2$ , in Fig. 4b between the times  $t = 12.1$  and  $12.2$ , and in Fig 4c between  $t = 28.0$  and  $28.1$ .

To summarize, the interaction between these shock systems shows attachment when the bars are aligned with each other and detachment when they are perpendicular. The shapes of the secondary shocks depend on the angle between the bars.

The most dramatic difference between the models comes from the gas evolution in the third region, deep inside the secondary bar. In Model 1, the gas settles within the central  $r \approx 0.02$  (i.e., 200 pc) where it experiences very little dissipation, compared to the outer shocks. In fact, we observe a kind of “limb brightening” at the edge of this bar. This is seen in Fig. 4a as an enhanced density of above-the-average dissipating particles outside the oval-shaped central region. The reason for this is that the gas joins the bar from all azimuths. In Model 2, the interior of the gaseous bar is uniformly dissipative at earlier times (Fig. 4b). The source of this dissipation is the small-scale shocks which are typically perpendicular to the major axis of the secondary bar. This is not the type of ‘centered’ shocks observed by Athanassoula (1992) as it uniformly encompasses the inner bar and the width of this dissipation zone is roughly equal to the minor axis of the bar. Note, that the dark shade here does *not* mean increased dissipation rate per particle, it only reflects the high density of the SPH particles. At later times, this dissipation rate decreases sharply (Fig. 4c).

We have looked more carefully into the central dissipation of Models 1 and 2 by using logarithmically grey-scaled maps (Figs. 5a,b). Both the “limb brightening” and the broad dissipation can be observed in detail. While some spatial dependency of the dissipation morphology can be seen in Fig. 5b of Model 2, no large-scale shocks are present.

#### 4. Discussion: Gas Dynamics in Nested vs Single Bars

This paper deals with the gas flow in dynamically-decoupled nested bars, focusing on two central issues, namely (i) is the gas capable of crossing the bar-bar interface in the nested bar systems, and (ii) do offset dust lanes form in the secondary bars. We first comment on the principal differences between the flow in the *single* large-scale bars and in the *nested* bars.

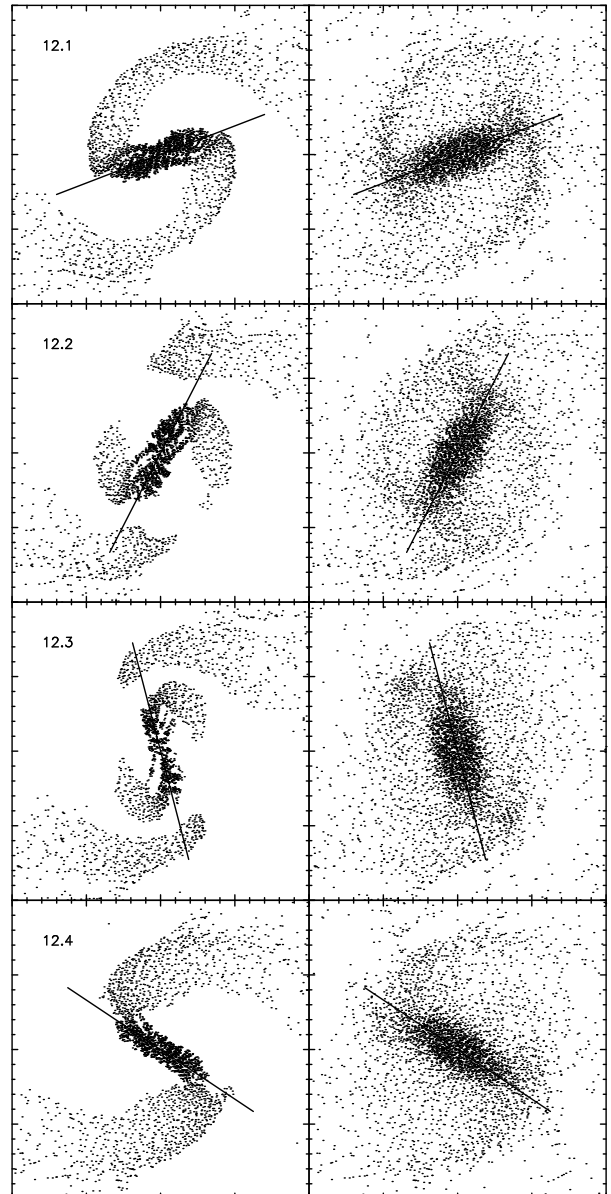


Fig. 4b.— Pattern of shock dissipation (left) and density evolution (right) in the central kpc ( $r = 0.1$ ) of Model 2 at early times, shown in the frame of reference of the primary bar (horizontal). Position of the secondary bar and its length are indicated with a straight line. All rotation is counter-clockwise. The particles on the left are those having greater than average dissipation rate which is given by the time derivative of the nonadiabatic component of internal energy. Note the broadly shocked region of the bar in the innermost 0.05. Also visible are two dissipative systems associated with the large-scale shocks in the primary bar and with the trailing shocks in the secondary bar.



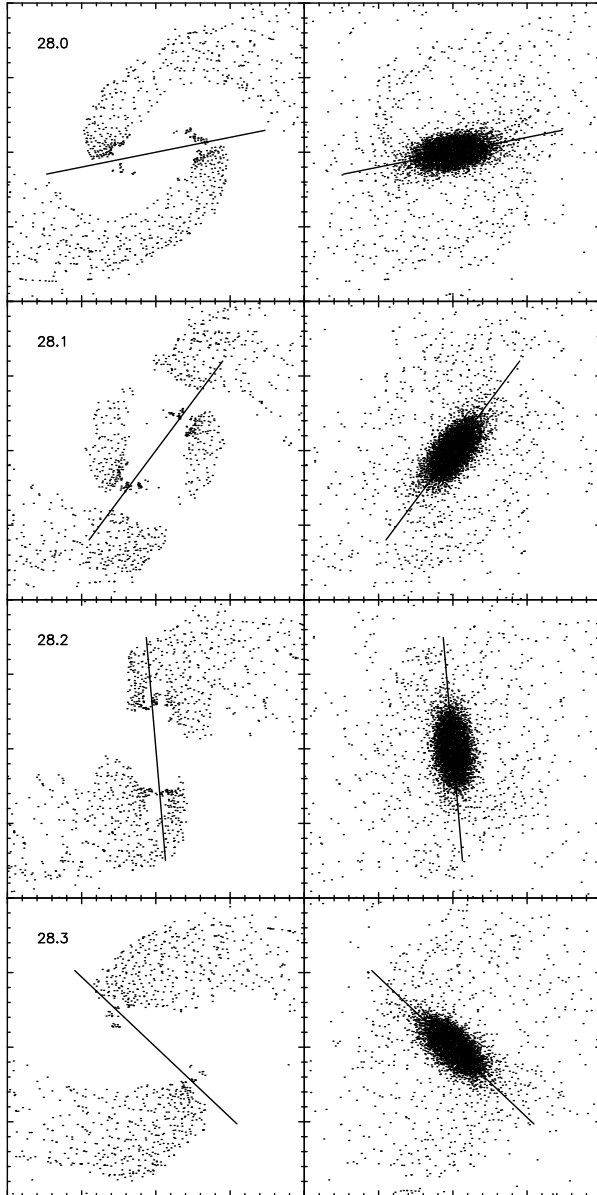


Fig. 4c.— Pattern of shock dissipation (left) and density evolution (right) in the central kpc ( $r = 0.1$ ) of Model 2, shown at late times. See Fig. 4b caption for further details.

#### 4.1. Gas flow across the bar-bar interface

In the presence of only one bar with a double ILR, the gas accumulates between the resonances in the form of two nuclear rings, as a result of shock focusing. These rings may or may not merge due to hydrodynamical interaction, depending on the width of the resonance region, shape of the underlying potential and the level of star formation, unrelated to

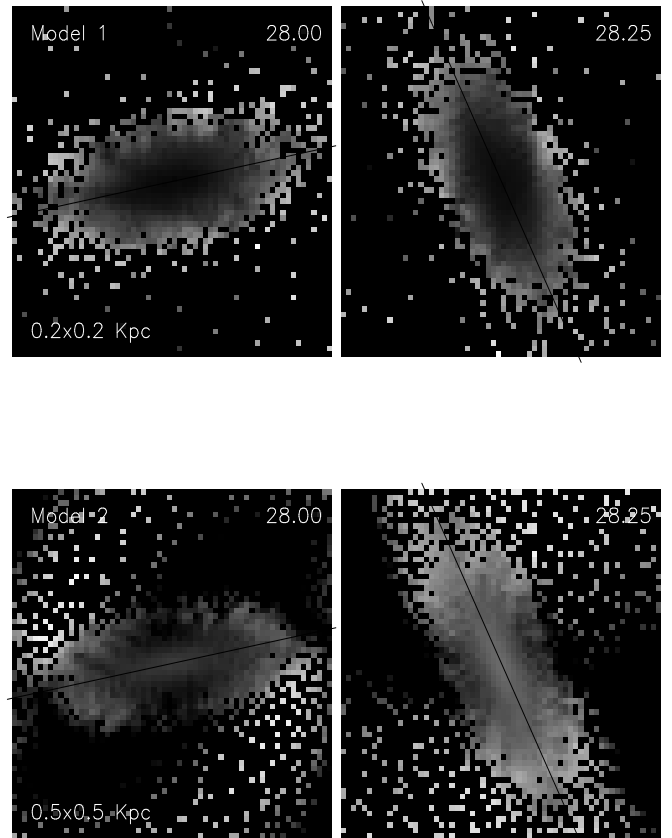


Fig. 5.— Logarithmic grey-scale map of shock dissipation in the interior of the secondary bar aligned at two different angles with respect to the primary bar (horizontal): (a) Model 1 (the inner 0.02), (b) Model 2 (the inner 0.05). The grey level is the logarithm of the viscous dissipation rate averaged over a pixel and scaled between 0.01 – 1.0 of the maximum rate, i.e., darker colors represent less dissipation. It is given by the time derivative of the nonadiabatic component of internal energy. The orientation of the secondary bar is given by the solid line. All rotation is counter-clockwise.

the importance of gas self-gravity. The slowdown of gas evolution at the resonances has been known for some time. Past numerical simulations (e.g., Combes & Gerin 1985; Piner, Stone & Teuben 1995), however, did not catch the possibility of a non-self-gravitational dynamical runaway which can develop in the nuclear rings (Heller, Shlosman & Englmaier 2001). With self-gravity, the gas accumulation near the ILRs is subject to global instabilities, and fur-

ther inflow is expected to be accompanied with star formation (Knapen et al. 1995b; Shlosman 2001).

As argued by Pfenniger & Norman (1990), the gas flow in nested bars has difficulty in crossing the bar interface, being repelled there unless self-gravitational effects in the gas develop. One can understand this by noting that the effective potential shape corresponds to a rim at the bar corotation from which the gas is forced to move away, both inwards or outwards. Our modeling shows that the gas flow, in fact, has no difficulty in crossing this resonance, and that this crossing is facilitated by the large-scale shocks which penetrate the region (roughly) along the minor axis of the primary bar, as shown in Figs. 4. We do observe a relatively insignificant outflow along the major axis of the primary bar, just outside the corotation of the small bar. But this outflow is completely offset by the inflow along the large-scale shocks of the main bar, coming in along the minor axis of the bar. This phenomenon was not captured by the “axisymmetric” analysis of Pfenniger & Norman.

The flow in single and double bars is found to be remarkably similar *outside* the bar-bar interface zone in all three models. This similarity, however, ends at the interface. Model 3 forms a nuclear ring made up of tightly wound spiral shocks and very little action takes place inside this ring. Model 1, with the short secondary bar, forms a similar ring which apparently is able to survive the perturbing action of the small bar. Note that the ring radius is about 0.04–0.05, and sits just at the bar edge, well inside its corotation. In contrast, the nuclear ring is being constantly disrupted and is not present most of the time in Model 2, in which the small bar extends close to its own corotation. Except when the bars are nearly aligned, the inner bar is situated in a disk-like envelope of gas, e.g., at times  $t = 12.2$  and  $12.3$  in Fig. 4b. The incoming large-scale shocks are most prominent when the bars are aligned and disappear at other angles.

An important observational corollary is that nuclear rings are expected to be absent in decoupled nested bars, unless the secondary bars are very centrally concentrated and/or short compared to their corotation.

The shape of the gas response inside the small bar also differs between the models. Model 1 exhibits a small gaseous bar of about 1/3 of the imposed stellar potential, and the shape is elliptical at all times (Fig. 4a). The gas is unable to settle down in the outer part of the bar due to the time dependent grav-

itational potential there. In addition, the characteristic diagram for this bar (Fig. 1b) has unstable and intersecting  $x_1$  orbits for  $r > 0.03$ , and so the subsequent gas behavior comes as no surprise.

In Model 2, the evolution is more complicated as the  $x_1$  orbits are stable but the variability of the gravitational potential is more severe. In the early stage of the gas inflow, it is filling up to 90% of the secondary bar, and the shape of the gaseous bar changes from being oval to rectangular (when it leads the primary bar by about  $45^\circ$ ) (Fig. 4b). This shape corresponds to the shape of the outer orbits in the small bar, close to its Ultra-harmonic resonance. At later times, the gaseous bar is about half of the size of the secondary bar background potential and its shape is oval as in the Model 1.

#### 4.2. Absence of offset grand-design shocks in secondary bars

Numerical simulations presented here demonstrate that the gas dynamics of the decoupled secondary bars differs substantially from that of the primary or single bars. A number of factors contribute to this, the first of which is the time-dependent nature of the gravitational potential in the nested bar system due to the distinct rates of bar tumbling during the dynamically-decoupled phase. The second factor is the gas injection into the secondary bar which proceeds through the primary large-scale shocks penetrating the bar-bar interface. No such phenomenon is operating across the corotation of the primary bars, which is rather depopulated of gas. The above factors are accompanied by a large amount of dissipation and the subsequent inability of the gas to settle in the outer half of the secondary bar. This raises the interesting question of whether secondary bars extend to their corotation, as their large-scale counterparts are believed to do. Based on the numerical simulations, we infer that secondary bars are more centrally concentrated than primary or single bars, and that the gas distribution in these bars does not extend to their corotation radii. Even if the  $x_1$  orbits can, in principle, be found at energies close to the Ultra-harmonic resonance, in many cases they are unstable, self-intersect and are unable to trap regular orbits around them. These orbits cannot support the gaseous component as well.

The third factor which differentiates the secondary from other type of bars is their fast pattern speed which does not allow for secondary ILRs to form in-

side the bar. If the decoupled phase of nested bars is short-lived, the quadrupole interaction between the bars will not be able to brake the small bar and form the ILRs. However even in the case of a long-lived decoupled phase we do not expect the nuclear bars to slow down. In fact, the gas inflow across the interface and the resulting central concentration speed up the bar, as can be inferred from numerical experiments with Sticky Particles (Shlosman & Noguchi 1993) and SPH (Heller & Shlosman 1994) hydrocodes. Because of the fast rotation, the  $x_1$  orbits deep inside the secondary bars are round, with no end-loops or needle shapes. As noted by Athanassoula (1992), for the shocks to exist, the curvature of the  $x_1$  orbits at apocenters must be sufficiently large, or they must have end-loops. The low Mach number gas flow is well organized here and capable of following these orbits with little dissipation, as shown in Figs. 4b,c.

Indeed, the nonlinear orbit analysis (Fig. 1) shows that the main orbits aligned with the secondary bar,  $x_1$  have a mild ellipticity and no end-loops. This result is rather robust and holds despite the extreme axial ratio, 4 : 1, used here. No offset large-scale shocks form under these conditions and hence no offset dust lanes are expected either.

Hence, it is highly probable that decoupled secondary bars avoid their ILRs because of their high pattern speeds. When the ILRs are absent in a large-scale bar, the offset shocks weaken and recede to the major axis of the bar becoming “centered” (e.g., Athanassoula 1992). They do not disappear completely because the underlying stellar periodic orbits have either end-loops, are pointed, or have large curvature at the ends, forcing the gas to shock there. These orbital shapes result from the slower rotation of large bars compared to the nuclear ones. Despite the fact that such weak centered shocks can exist theoretically, only two examples have been found out of more than a hundred barred galaxies analyzed by Athanassoula (1992), one of which is the dubious case of NGC 7479. During the last decade only one more potential example has been added to this list (Athanassoula, private communication). We conclude that centered shocks are very rarely observed, possibly because of being so weak.

No ‘classical’ centered shocks have been observed in our numerical simulations. Instead we find that the inner half of the secondary bars show a rather uniform dissipation during the early stages of the gas inflow (Fig. 4b), which then sharply decreases at lat-

ter times (Figs. 4c, 5a,b). This dissipation is always small compared to dissipation in the primary large-scale shocks. It is interesting that a nuclear Lindblad resonance introduced by a central supermassive black hole should in principle lead to trailing spiral shocks, but at very small radii,  $\sim 10 - 50$  pc (Shlosman 1999; 2001).

It is important that both short and long (with respect to their corotation) nuclear bars show basically the same distribution of the gas component. The bar-bar interface (i.e., nuclear bar corotation) is almost always depopulated of gas because of the absence of non-intersecting orbits there. This conclusion holds for gas-dominated and star-dominated nuclear bars and has interesting implications which will be discussed elsewhere.

Knapen et al. (1995b) have analyzed the shock dissipation in a self-consistent gravitational potential of ‘live’ stars and gas *before* the decoupling phase, when both bars tumble with the same pattern speeds, and when the gas self-gravity is accounted for. No offset shocks have been found in this configuration either. Dust lanes, therefore, cannot be used to search for nuclear bars, as proposed by Regan & Mulchaey (1999) and Martini & Pogge (1999). Furthermore, the alternative method of NIR isophote fitting — a reliable approach in detecting large-scale bars, has its own difficulties when applied to nuclear bars. This has been shown by Laine et al. (2001) for the largest to-date matched sample of 112 Seyferts and non-Seyferts. The main difficulty in fitting the isophotes comes from localized and distributed sites of star formation, especially pronounced within the central kpc. This results in a substantial underestimate of the nuclear bar fraction and cannot be used reliably in order to analyze e.g., the role of nuclear bars in fueling of active nuclei. However, recent work by Martini et al. (2001), without invoking a matched control sample, is doing just this. Clearly, the most promising method in detecting the nuclear bars is 2D spectroscopy of the central kpc revealing the underlying kinematics.

An important issue is the fate of the gas accumulating in the inner parts of the secondary bars. Under the observed conditions in our numerical simulations (gas masses and surface densities) the gas self-gravity should have a dominating effect on its evolution. Shlosman (2001) has described the work of Englmaier & Shlosman (1999, unpublished) who studied the dynamical stability of nuclear rings under similar conditions and found that global self-gravitational

modes with  $m = 2$  and 4 are rapidly amplified into the non-linear regime. The gas loses its rotational support and falls towards the center, feeding the central supermassive black hole at peak rates and increasing their mass tenfold. Of course a big unknown is the concurrent star formation, which was neglected in these simulations. We note, however, that the star formation is unknown anywhere to reach so high an efficiency, that it would be able to halt this runaway collapse to the center. Clearly, conditions obtained at the end of our present numerical simulations of gas flow in nested bars are extreme and will be destabilized by the self-gravitational instabilities which will extract angular momentum from the gas on a dynamical timescale. It is important, therefore, that a ‘live’ gravitational potential of the bars immersed in the disk be used in order to get a qualitative and quantitative picture of further evolution in the central kpc of disk galaxies.

We conclude that no large-scale shocks and consequently no offset dust lanes will form inside secondary nuclear bars either when they are dynamically coupled and spin with the same pattern speeds as the primary bars, or dynamically decoupled, spinning much faster. Two main factors, the time-dependent gravitational potential and the nature of the gas flow deep inside the bar, prevent the formation of these dust lanes. The time-dependent, “anisotropic” gas inflow across the ILR/corotation interface found here is a completely new phenomenon inherent to nested bars, because in the single barred systems, no such inflow is possible at all *when the gas accumulation is small and its self-gravity is negligible*. The fate of the gas settling inside the nuclear bars cannot be decided without invoking global self-gravitational effects in the gas which will completely change the nature of the flow there. Star formation most probably will play an important role here, but because of its expected low efficiency, it is doubtful it would be capable of halting the inflow.

We thank Lia Athanassoula and Peter Englmaier for numerous discussions and the organizers of INAOE workshop on *Disk Galaxies: Kinematics, Dynamics and Perturbations* for supporting a prolonged visit during which this work was concluded. Supported in part by NASA grants NAG 5-10823, NAG 5-3841, WKU-522762-98-6 and HST GO-08123.01-97A to I.S.

## REFERENCES

- Athanassoula, E. 1992, MNRAS, 259, 345  
Athanassoula, E. 1994, in *Mass-Transfer Induced Activity in Galaxies*, ed. I. Shlosman  
Binney, & Tremaine, S. 1987, *Galactic Dynamics*, Princeton Univ. Press  
Buta, R. & Crocker, D.A. 1993, AJ, 105, 1344  
Combes, F. 1994, *Mass-Transfer Induced Activity in Galaxies*, ed. I. Shlosman (Cambridge Univ. Press), 170  
Combes, F. & Gerin, A. 1985, A&A, 150, 327  
Contopoulos & Papayannopoulos, 1980,  
de Vaucouleurs, G. 1974, *The Formation & Dynamics of Galaxies*, IAU Symp. 58, J. Shakeshaft, ed. (Reidel, Dordrecht), p. 335  
Devereux, N.A., Kenney, J.D.P. & Young, J.S. 1992, AJ, 103, 784  
Englmaier, P. & Gerhard, O. 1997, MNRAS, 287, 57  
Englmaier, P. & Shlosman, I. 2000, ApJ, 528, 677  
Erwin, P. & Sparke, L.S. 1999, ApJ, 521, L37  
Ferrers, N.M. 1877, Q.J. Pure Appl. Math., 14, 1  
Friedli, D. 1999, *Evolution of Galaxies on Cosmological Timescales*, J.E. Beckman & T.J. Mahoney, eds. (ASP Conf. Series)  
Friedli, D. & Martinet, L. 1993, A&A, 277, 2  
Friedli, D., Wozniak, H., Rieke, M., Martinet, L. & Bratschi, P. 1996, A&AS, 118, 461  
Hasan H., Norman C.A. 1990, ApJ, 361, 69  
Heller, C.H. & Shlosman, I. 1994, ApJ, 424, 84  
Heller, C.H. & Shlosman, I. 1996, ApJ, 471, 143  
Heller, C.H. & Shlosman, I. & Englmaier, P. 2001, ApJ, 553, 661  
Ishizuki, S., Kawabe, R., Ishiguro, M., Okumuro, S.K. & Morita, K.-I. 1990, Nature, 344, 244  
Jungwiert, B., Combes, F. & Axon, D.J. 1997, A&AS, 125, 479  
Knapen, J.H., Shlosman, I. & Peletier, R.F. 2000, ApJ, 529, 93  
Knapen, J.H., Beckman, J.E., Heller, C.H., Shlosman, de Jong, R.S. 1995, ApJ, 454, 623  
Kormendy, J. 1983, *Morphology and Dynamics of Galaxies*, 12th Advanced Course, Saas-Fee, Observatoire de Geneve, p. 113  
Laine, S., Shlosman, I., Knapen, J.H. & Peletier, R.F. 2001, ApJ, submitted

- Maciejewski, W. & Sparke, L.S. 2000, MNRAS, 313, 745
- Maiolino, R., Alonso-Herrero, A., Anders, S., Quillen, A., Rieke, M.J., Rieke, G.H. & Tacconi-Garman, L.E. 2000, ApJ, 531, 219
- Martini, P. & Pogge, R.W. 1999, AJ, 118, 2646
- Martini, P., Pogge, R.W. Ravindranath, S. & An, J.H. 2001, ApJ, November 10, in press
- Miyamoto, M. & Nagai, R. 1975, Publ. Astron. Soc. Japan, 27, 533
- Patsis, P.A. & Athanassoula, E. 2000, MNRAS, 358, 45
- Pfenniger, D. & Norman, C.A. 1990, ApJ, 363, 391
- Piner, B.G., Stone, J.M. & Teuben, P.J. 1995, ApJ, 449, 508
- Regan, M.W. & Mulchaey, J.S. 1999, AJ, 117, 2676
- Sakamoto, K., Baker, A.J. & Scoville, N.Z. 2000, ApJ, 533, 149
- Sandage, A. & Brucato, R. 1979, AJ, 84, 472
- Scoville, N.Z., Matthews, K., Carico, D.P. & Sanders, D.B. 1988, ApJ, 327, L61
- Shaw, M.A., Axon, D.J., Probst, R. & Gatley, I. 1995, MNRAS, 274, 369
- Shaw, M.A., Combes, F., Axon, D.J. & Wright, G.S. 1993, A&A, 273, 31
- Shlosman, I. 2001, *The central Kpc of Starbursts and AGNs*, J.H. Knapen et al., eds. (ASP Conf. Series), in press
- Shlosman, I. 1999, *Evolution of Galaxies on Cosmological Timescales*, J.E. Beckman & T.J. Mahoney, eds. (ASP Conf. Series), p. 100
- Shlosman, I. 1996, in Proc. Centennial Nobel Symp. on *Barred Galaxies & Circumnuclear Activity*, Aa. Sandqvist & P.O. Lindblad, Eds. (Springer-Verlag), p. 141
- Shlosman, I. & Noguchi, M. 1993, ApJ, 414, 474
- Shlosman, I., Begelman, M.C. & Frank, J. 1990, Nature 345, 679
- Shlosman, I., Frank, J. & Begelman, M.C. 1989, Nature 338, 45